https://doi.org/10.5194/egusphere-2026-5126
Preprint. Discussion started: 10 September 2026

Elevated shortwave radiation enhances the limitation of atmospheric dryness on carbon sequestration across European forests

Ziqian Zhong[1], Hans W. Chen[1,*], Fuxiao Jiang[2], Luyao Liu[3, 4]

[1]Department of Environmental and Energy Sciences, Division of Geoscience and Remote Sensing, Chalmers University of Technology, SE-412 96 Gothenburg, Sweden
[2]Institute of Earth Surface Dynamics (IDYST), UNIL-Mouline, Geopolis, Office 3141, University of Lausanne, 1015 Lausanne, Switzerland
[3]Key Laboratory of Forest Ecology and Management, Institute of Applied Ecology, Chinese Academy of Sciences, Shenyang 110016, China
[4]TUM School of Life Sciences, Technical University of Munich, Freising 85354, Germany

*e-mail: hans.chen@chalmers.se

Abstract

Since the 1980s, both incoming shortwave radiation (SW) and atmospheric vapor pressure deficit (VPD) have increased significantly across Europe and are projected to continue rising in the coming decades, potentially altering forest photosynthesis and carbon storage. However, the joint impacts of SW and VPD on forest carbon sequestration remain poorly understood. Here, using half-hourly flux tower observations combined with remotely sensed vegetation indices, we show that SW and VPD are the dominant energy- and water-related drivers of forest net ecosystem exchange (NEE; negative values indicate net carbon uptake) at the half-hourly scale across Europe. We identify two thresholds in the VPD–NEE relationship. For VPD values below 3.90 hPa, the influence of VPD on NEE is weakly negative. Above this threshold, VPD's effect on NEE increases approximately linearly, shifting from negative to positive as VPD rises. A second threshold is detected at 20.84 hPa, beyond which the effect of VPD continues to increase but at a slower rate. The influence of VPD on NEE is strongly mediated by SW, with the sensitivity of NEE to VPD increasing more steeply under high SW conditions than under low SW conditions. This pattern is consistent with stronger stomatal limitation under high-radiation conditions, thereby suppressing photosynthesis and altering NEE. Together, these findings suggest that future increases in atmospheric dryness—potentially

https://doi.org/10.5194/egusphere-2026-5126
Preprint. Discussion started: 10 September 2026

reinforced by continued brightening—may substantially constrain forest productivity and carbon sequestration in Europe. Our results underscore the importance of accounting for SW–VPD interactions in climate impact assessments and forest management strategies.

Keywords: forest, carbon sequestration, VPD, shortwave radiation, Europe

1. Introduction

The carbon balance of terrestrial ecosystems is highly sensitive to climate change (Piao et al., 2008), particularly to shifts in climatic drivers of plant production. One notable trend in recent decades is the widespread decline in solar radiation from the 1950s to the 1980s (Stanhill and Cohen, 2001; Wild, 2009), followed by a marked increase in surface solar radiation—commonly referred to as "brightening" (Wild et al., 2005; Wild, 2009)—since the mid-1980s, especially in some regions such as Europe (Sanchez-Lorenzo et al., 2017; Pfeifroth et al., 2018). In addition, the increase in atmospheric vapor pressure deficit (VPD) associated with persistent global warming has contributed to higher atmospheric evaporative demand and intensified drought severity in recent decades (Fang et al., 2022; Zhong et al., 2025b; Gebrechorkos et al., 2025). Changes in these climatic factors are likely to exert strong influences on ecosystem productivity and carbon fluxes and storage, acting independently or through synergistic or antagonistic interactions (Lindner et al., 2010).

Forests occupy roughly one-third of Europe's land area and provide essential ecosystem services, including carbon sequestration, water filtration, and soil protection, while also buffering human infrastructure against natural hazards (Patacca et al., 2023; Senf and Seidl, 2021; Seidl et al., 2014). It has long been recognized that forest productivity and mortality in Europe are closely linked to soil drought, mainly driven by precipitation deficits (Ciais et al., 2005; Senf et al., 2020; Carnicer et al., 2011; Beloiu et al., 2022). However, mounting evidence highlights the previously underestimated role of atmospheric dryness. Elevated VPD typically triggers partial stomatal closure to limit water loss and prevent excessive xylem tensions from reaching critical thresholds that could cause cavitation and hydraulic failure, thereby reducing photosynthesis and carbon assimilation (Mcdowell et al., 2018; Song et al., 2022). Forest growth in certain regions such as

https://doi.org/10.5194/egusphere-2026-5126
Preprint. Discussion started: 10 September 2026

Central Europe (Trotsiuk et al., 2021), and in species such as beech (Lendzion and Leuschner, 2008; Sanginés De Cárcer et al., 2018), is strongly constrained by elevated VPD. Importantly, VPD-related stress can occur even when soil moisture is not limiting, for example, during the European summer drought of 2018 (Fu et al., 2020). High VPD has also been identified as the dominant driver of reduced gross primary production (GPP) in southern and central Europe during July–August 2022 (Van Der Woude et al., 2023). While numerous studies have examined the VPD effects on vegetation productivity (Wang et al., 2022; Xie et al., 2024; Zhang et al., 2024; Lin et al., 2025), considerably less is known about its influence on ecosystem-scale carbon exchange. Moreover, the VPD thresholds at which atmospheric dryness begins to strongly suppress forest carbon exchange remain poorly quantified.

Solar radiation is fundamental to forest productivity as it fuels photosynthesis, which generates the assimilates used by trees to form new wood tissue (Hartmann and Trumbore, 2016; Rossi et al., 2016). However, intense solar irradiance also increases evapotranspiration and can induce drought stress and foliage damage. Recent dendrometer-based field observations in Central Europe indicate that high solar irradiance enhances the growth of temperate old-growth forests during long photoperiods, but suppresses growth via increased VPD and drought stress (Kašpar et al., 2024). Generally, increasing solar irradiance elevates leaf temperature above ambient air temperature, thereby raising VPD near the leaf surface. High solar radiation can also amplify atmospheric evaporative demand, intensifying plant water stress (Mokhtari et al., 2018; Bois et al., 2008). Despite these known interactions, the extent to which solar radiation modulates VPD effects on stomatal behavior—and consequently on vegetation productivity and carbon uptake—remains insufficiently understood. Moreover, as high-VPD and high-radiation conditions are expected to become increasingly common under continued warming (Xu et al., 2023a; Van Der Woude et al., 2023; Fang et al., 2022) and brightening (Gutiérrez et al., 2020; Hou et al., 2021) in Europe, disentangling their individual and combined influences on tree productivity and forest carbon exchange becomes critical for predicting future forest dynamics.

In this study, we combined half-hourly eddy-covariance flux tower observations from forest sites across Europe (Icos Ri et al., 2025) with an eXtreme Gradient Boosting model (Chen and Guestrin,

https://doi.org/10.5194/egusphere-2026-5126
Preprint. Discussion started: 10 September 2026

2016) and SHapley Additive exPlanations (Lundberg et al., 2020)—referred to here as XGBoost-SHAP—to explore the effects of environmental factors and their interactions on net ecosystem carbon exchange (NEE, where negative values denote net ecosystem carbon uptake) across European forests. We also employed path analysis to quantify the direct and indirect relationships between environmental variables and NEE. Finally, we evaluated the response of ecosystem conductance (G_s) to VPD to clarify the role of atmospheric dryness and solar radiation in regulating forest productivity.

2. Data and methods

2.1 Data

This study used flux tower measurements from European forests (Icos Ri et al., 2025), complemented by remotely sensed leaf area index (LAI) data. The half-hourly tower observations include incoming shortwave radiation (SW), vapor pressure deficit (VPD), air temperature (TA), soil water content (SWC), precipitation (P), wind speed (WS), and NEE (NEE_VUT_REF), as well as estimated GPP from daytime (GPP_{DT}, GPP_DT_VUT_REF) and nighttime (GPP_{NT}, GPP_NT_VUT_REF) partitioning methods. These variables were obtained from the Integrated Carbon Observation System (ICOS) as the Ecosystem final quality (L2) product in ETC-Archive format (release 2025-1) (Icos Ri et al., 2025). Surface-layer SWC was used, as it was available for most ICOS sites. For each year, only data from the main growing season (May–October) (Jeong et al., 2012; Xu et al., 2023b) were included. Years with less than 5% missing values during the main growing season were included in the analysis. Furthermore, only time series containing complete observations for at least three years of growing-season data were selected for analysis. A total of 23 sites were selected where all required variables were available (Fig. 1, Table S1), including 6 deciduous broadleaf forest (DBF) sites, 1 deciduous needleleaf forest (DNF) site, 1 evergreen broadleaf forest (EBF) site, 13 evergreen needleleaf forest (ENF) sites, and 2 mixed forest (MF) sites. Most data (92.05%) were collected between 2019 and 2024, providing an up-to-date understanding of forest carbon uptake in response to climate variability and change while minimizing potential confounding effects from long-term physiological adjustments of

https://doi.org/10.5194/egusphere-2026-5126
Preprint. Discussion started: 10 September 2026

photosynthesis and respiration, such as thermal acclimation (Way and Yamori, 2014; Wu et al., 2025). Only daytime observations were analyzed, as the effects of SW and VPD on ecosystem carbon exchange primarily occur during the day. Daytime and nighttime were distinguished using the variable "NIGHT" provided in the dataset, which is derived from potential (top of atmosphere) incoming shortwave radiation. LAI data were obtained from the MCD15A3H product (Myneni et al., 2015) at the flux tower sites with a spatial resolution of 1 km and a temporal resolution of 4 days. In the analysis, LAI values were assigned to half-hourly time steps based on the temporally closest observation.

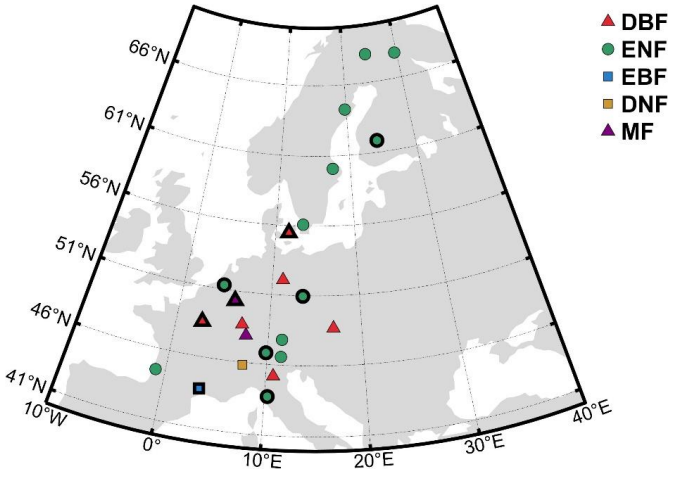

Fig. 1. Spatial distribution of flux tower sites. The ecosystems include evergreen needleleaf forest (ENF), deciduous needleleaf forest (DNF), evergreen broadleaf forest (EBF), deciduous broadleaf forest (DBF) and mixed forest (MF). Sites used for the analysis of the ecosystem conductance–VPD relationship are marked with thicker borders around the symbols.

To investigate the relationship between G_s and VPD, measurement height and canopy height data were obtained for 9 flux tower sites from Wang et al. (2020). The sites (Fig. 1, Table S1), which provide continuous observations of outgoing shortwave radiation, incoming and outgoing longwave radiation, soil heat flux and latent heat flux, were further selected for the analysis of the G_s–VPD relationship.

https://doi.org/10.5194/egusphere-2026-5126
Preprint. Discussion started: 10 September 2026

2.2 XGBoost-SHAP framework

We applied the XGBoost algorithm to simulate forest carbon fluxes and quantify the contributions of climatic drivers. XGBoost is a scalable ensemble learning method based on gradient-boosted decision trees (Chen and Guestrin, 2016) and is widely used for nonlinear regression due to its strong predictive performance and ability to handle multicollinearity among predictors (Wang et al., 2022; Xie et al., 2024). To interpret the XGBoost model, we employed SHAP, a game-theoretic framework that attributes predictions to individual features (Lundberg et al., 2020). SHAP values quantify each predictor's marginal contribution while capturing nonlinear effects and pairwise interactions.

Half-hourly TA, SW, P, WS, VPD, SWC, and LAI were used as predictors, and NEE or GPP served as the target variable, depending on the analysis. After omitting missing values, the dataset was randomly split into training (80%) and validation (20%) subsets. The XGBoost regression models were trained with squared-error loss with 100 boosting iterations. Model performance was evaluated on the validation set using the coefficient of determination (R^2). SHAP values were computed using the TreeExplainer framework applied to the trained model and the validation data. We used SHAP dependence plots to examine the direction and magnitude of predictor effects, and SHAP interaction values to identify and quantify pairwise interactions among predictors.

2.3 Threshold analysis

Based on the SHAP response curves, we fitted a continuous piecewise linear model to describe the relationship between VPD and its SHAP values. To justify the number of segments, we compared one- to four-segment models using the VPD SHAP response for NEE. The raw-data coefficient of determination (R^2) increased from 0.70 to 0.83, 0.85, and 0.85 for the one-, two-, three-, and four-segment models, respectively. Because the improvement from three to four segments was marginal, we selected the three-segment model based on the principle of parsimony. Before model fitting, paired VPD–SHAP observations were sorted by VPD and grouped into equally spaced bins across the predefined VPD range. The model was then fitted to these binned median responses by minimizing a weighted residual sum of squares. The fitted function is defined as:

https://doi.org/10.5194/egusphere-2026-5126
Preprint. Discussion started: 10 September 2026

$$f(x) = \begin{cases} \beta_0 + \beta_L(x - \tau_1), x \le \tau_1 \\ \beta_0 + \beta_I(x - \tau_1), \tau_1 < x \le \tau_2 \\ \beta_0 + \beta_I(\tau_2 - \tau_1) + \beta_H(x - \tau_2), x > \tau_2 \end{cases} \quad (1)$$

The fitted function consisted of three continuous linear segments connected by two thresholds, denoted as τ_1 and τ_2. In this model, x represents VPD and $f(x)$ the corresponding SHAP value. The parameter β_0 represents the fitted SHAP value at τ_1, whereas β_L, β_I, and β_H describe the slopes of the low-, intermediate-, and high-VPD segments, respectively. Continuity was enforced at both thresholds so that the fitted response remained continuous across the full VPD range.

Model parameters were estimated by minimizing the residual sum of squares. The goodness of fit was evaluated using the R^2 between actual and fitted SHAP values. Uncertainty in threshold estimates was quantified using bootstrap resampling. Specifically, the original paired VPD–SHAP observations were resampled with replacement 10,000 times while preserving the original sample size in each replicate. For each bootstrap sample, the full fitting procedure was repeated, including binning, calculation of median SHAP values, weighted fitting of the three-segment piecewise model, and estimation of τ_1 and τ_2. This yielded empirical distributions of the two threshold estimates, from which the 2.5th and 97.5th percentiles were taken as the lower and upper bounds of the 95% confidence interval.

2.4 Path analysis

To disentangle the multiple pathways through which VPD and its interactions with other variables affect NEE, we employed a covariance-based structural equation model (CB-SEM). CB-SEM is a multivariate statistical technique that quantifies both direct and indirect effects among variables while incorporating prior knowledge to establish hypothesized causal relationships. It is particularly useful for testing complex theoretical frameworks, as it enables the simultaneous estimation of multiple pathways. The theoretical foundations for the hypothesized pathways in this study (Fig. 2) are as follows: (1) SW directly drives photosynthesis, which regulates vegetation productivity and NEE. (2) SWC determines the water availability for trees (Liu et al., 2020). Low SWC is a well-established indicator of drought stress and reflects its impacts on productivity and NEE (Stocker et al., 2018). (3) TA regulates key physiological processes, including photosynthesis, respiration,

https://doi.org/10.5194/egusphere-2026-5126
Preprint. Discussion started: 10 September 2026

transpiration, and cell development, thus directly influencing NEE (Huang et al., 2019; Chen et al., 2023b; Körner, 2003). (4) VPD controls stomatal behavior, affecting photosynthesis and forest productivity. Under high VPD, reduced stomatal conductance suppresses photosynthesis, leading to higher (more positive) NEE (Yuan et al., 2019; He et al., 2021; Zhong et al., 2023b). (5) These environmental drivers interact: SW is partly absorbed at the Earth's surface and converted into heat, thereby increasing TA; according to the Clausius–Clapeyron relationship (Murray, 1967; Buck, 1981), higher TA strongly elevates saturated vapor pressure and thus VPD (Xu et al., 2025); SWC is often negatively correlated with VPD due to land–atmosphere interactions (Seneviratne et al., 2010; Zhou et al., 2019); SW and TA enhance evapotranspiration (Donohue et al., 2010), thereby influencing SWC; soil moisture can influence SW availability through cloud formation (Ek and Holtslag, 2004); and the evaporative cooling effect of SWC can moderate TA (Dai et al., 1999).

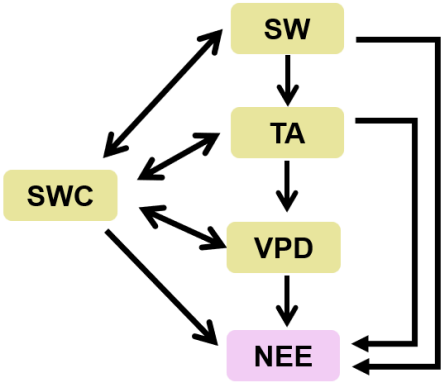

Fig. 2. Hypothesized relationships among environmental variables influencing NEE Single-headed arrows denote hypothesized directional pathways, whereas double-headed arrows denote covariances.

All variables were standardized to z-scores prior to the path analysis. Model parameters were estimated using maximum likelihood, and model fit was assessed using multiple indices (Zhong et al., 2025a), including the comparative fit index (CFI), adjusted goodness-of-fit index (AGFI), and root mean square error of approximation (RMSEA). Predictor effects were quantified as standardized influence coefficients from the CB-SEM, with larger positive values indicating

https://doi.org/10.5194/egusphere-2026-5126
Preprint. Discussion started: 10 September 2026

stronger effects. Direct effects were represented by path coefficients, which capture the direction and magnitude of relationships, while indirect effects reflect the influence of a predictor on a response variable through intermediate pathways (Zhong et al., 2023b).

2.5 G_s and G_s–VPD relationship

Given that VPD effects on vegetation largely operate through stomatal regulation, we examined how SW modulates the relationship between VPD and G_s, which integrates canopy and soil conductance and is commonly used as a proxy for stomatal regulation at the ecosystem scale. When stomata close in response to atmospheric dryness, transpiration declines and G_s correspondingly decreases. Here, G_s was estimated by inverting the Penman–Monteith equation (Penman and Long, 1963; Penman, 1948):

$$[G_s] = \frac{\gamma \times g_a \times LE}{\Delta \times (R_n - G - LE) + \rho C_p g_a VPD - \gamma LE} \quad (2)$$

where $[G_s]$ is the conductance (m s^{-1}), γ is the psychrometric constant (hPa K^{-1}), g_a is the aerodynamic conductance (m s^{-1}), LE is the latent heat flux (W m^{-2}), Δ is the slope of the saturated vapor pressure curve (hPa K^{-1}) as a function of temperature, R_n is the net radiation (W m^{-2}) calculated as the sum of incoming shortwave and longwave radiation minus the sum of outgoing shortwave and longwave radiation, G is the soil heat flux (W m^{-2}), ρ is the air density (kg m^{-3}), and C_p is the specific heat capacity of air taken as 1012 J kg^{-1} K^{-1}. Here, g_a was calculated as:

$$g_a = \frac{WS \times k^2}{[\ln((z_m - z_d)/z_o)]^2} \quad (3)$$

where WS is the measured wind speed (m s^{-1}), k is the von Karman constant (0.4), z_m is the measurement height, z_d is the zero-plane displacement, and z_o is the momentum roughness length. Following (Fu et al., 2022), z_d and z_o were taken as $0.67h$ and $0.1h$, respectively, where h is the canopy height.

The ideal gas law (Pearcy et al., 1989) was applied to convert $[G_s]$ from m s−1 to G_s in mol m^{-2} s^{-1}:

https://doi.org/10.5194/egusphere-2026-5126
Preprint. Discussion started: 10 September 2026

$$G_s = [G_s]\frac{P_a}{R \times TA} \quad (4)$$

where P_a is the atmospheric pressure (hPa) and R is the dry air gas constant (0.08314 m^3 hPa K^{-1} mol^{-1}). To reduce the influence of extreme values and more accurately quantify the dependence of G_s on VPD, we retained only G_s values within the 5th–95th percentile range and excluded observations from rainy days and the following day (Lin et al., 2018).

To characterize the relationship between G_s and VPD under different SW conditions, we applied a nonlinear regression approach. Specifically, G_s was modeled as a function of VPD using a simplified version of Equation (2):

$$G_s = \frac{a}{1 + b \times VPD} \quad (5)$$

where a and b are parameters to be estimated. The parameter values were obtained through nonlinear least-squares fitting (Marquardt, 1963), which minimizes the sum of squared differences between observed and predicted values.

3. Results

3.1. Environmental drivers of NEE

We first analyzed the effects of half-hourly environmental variables on NEE in European forest ecosystems. The XGBoost model was trained and optimized, achieving an R^2 of 0.72 on the validation set. SHAP values were then computed to quantify the contribution of each predictor to NEE across all samples and sites (Fig. 3). Positive SHAP values indicate that the given predictor value increases the predicted NEE relative to the model's base value (toward increasing carbon source), while negative values indicate that it decreases predicted NEE (toward increasing carbon sink). The relative importance of each predictor was further assessed using the normalized magnitude of its absolute SHAP values.

https://doi.org/10.5194/egusphere-2026-5126
Preprint. Discussion started: 10 September 2026

Among all predictors, SW had the highest relative SHAP importance, accounting for 61.1% of the total attribution magnitude. This is followed by VPD, LAI, and TA, which accounted for 15.4%, 8.0%, and 7.5% of the variability, respectively. Generally, higher values of these predictors were associated with less positive or more negative NEE, except for VPD (Fig. 3a). A similarly strong influence of SW and VPD on NEE was detected when the analysis was repeated using daily daytime averages, with SW and VPD accounting for 42.2% and 14.0% of the total mean absolute SHAP importance, respectively (Fig. S1a). These findings indicate that SW and VPD are the primary energy- and water-related controls of forest NEE at the half-hourly and daily scales.

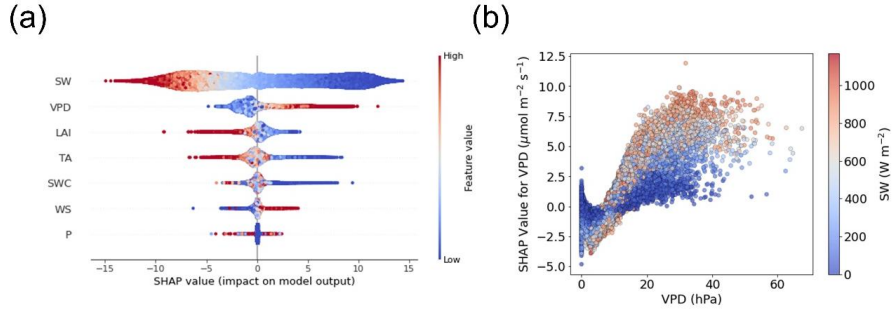

Fig. 3. SHAP values of net ecosystem carbon exchange (NEE) drivers. (a) SHAP summary bee swarm plots, where each dot represents a site-level half-hourly sample. When multiple dots overlap at the same x position, they accumulate to reflect density. Dot color indicates the feature value, with blue representing low values and red representing high values. (b) SHAP dependence plot showing the relationship between VPD and its SHAP values, stratified by the gradient of incoming shortwave radiation (SW). The XGBoost model achieved an R^2 of 0.72 on the held-out validation set.

We investigated how climatic drivers modulate the VPD–NEE relationship using SHAP dependence plots derived from the validation set, which capture coupling effects between predictors. At low VPD, SHAP values were near neutral, but they increased rapidly once VPD exceeded ~5 hPa. This suggests that VPD had a limited influence on photosynthesis below this threshold. However, once VPD exceeded this threshold, further VPD increases suppressed vegetation productivity, resulting in higher (more positive) NEE (Fig. 3b). A pronounced coupling effect between VPD and TA was evident: higher VPD was generally associated with higher TA, together producing positive SHAP values (Fig. S2b). By contrast, the coupling effect between VPD and SWC was weaker (Fig. S2c), indicating that elevated VPD tended to increase NEE across the full SWC range.

https://doi.org/10.5194/egusphere-2026-5126
Preprint. Discussion started: 10 September 2026

Interestingly, compared with the interaction between VPD and SWC, the interaction between VPD and SW was more pronounced (Fig. 3b). Under low SW conditions, SHAP values for VPD increased gradually after exceeding the threshold and remained relatively low, whereas under high SW conditions, they rose sharply. These results highlight the regulatory role of solar radiation in mediating the VPD effects on NEE. Additional analyses for the two dominant European forest types—DBF and ENF—revealed similar patterns, further underscoring the importance of SW in shaping the VPD–NEE relationship (Fig. S3).

Next, we assessed the effects of environmental factors and their interactions on both GPP_{DT} and GPP_{NT} using the XGBoost-SHAP framework (Fig. 4). Among all predictors, SW was the dominant driver, accounting for nearly 50% of the total mean absolute SHAP importance for both GPP_{DT} and GPP_{NT}. Consistent with its influence on NEE, VPD accounted for 12.2% and 14.1% of the variability in GPP_{DT} and GPP_{NT}, respectively. We also observed a regulatory role of SW in mediating the VPD–GPP relationship: under low SW conditions, SHAP values for VPD decreased gradually after exceeding the threshold, whereas under high SW conditions, they declined sharply. Overall, these analyses reinforce the key role of SW in shaping the relationship between VPD and forest productivity, as well as ecosystem carbon exchange.

https://doi.org/10.5194/egusphere-2026-5126
Preprint. Discussion started: 10 September 2026

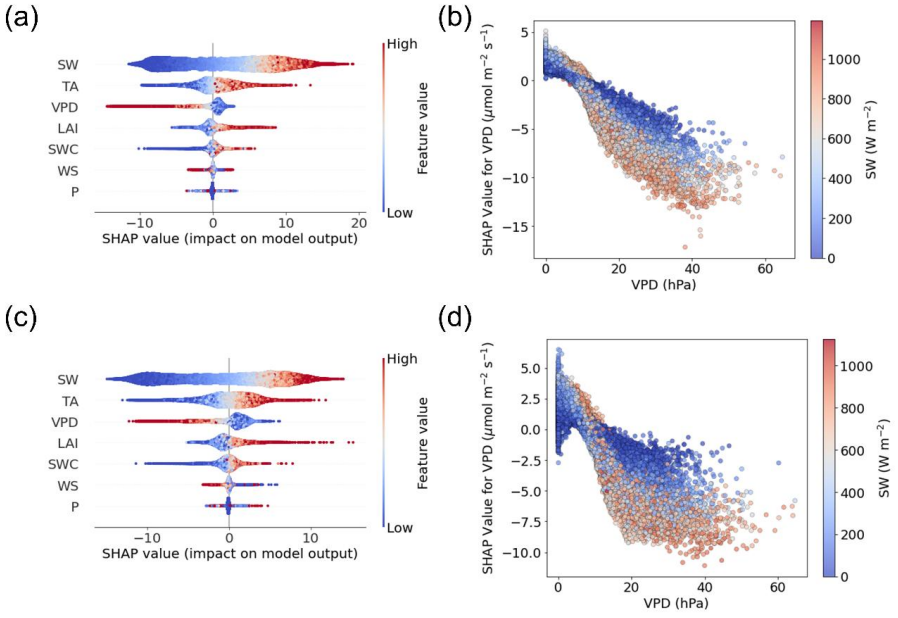

Fig. 4. SHAP values of gross primary production (GPP) drivers. (a) and (c), SHAP summary bee swarm plots showing predictor contributions to GPP from daytime (GPP_{DT}, a) and nighttime (GPP_{NT}, c) partitioning methods, where each dot represents a site-level half-hourly sample. The x-axis position indicates the contribution of a given variable to the XGBoost model prediction for that sample. When multiple dots overlap at the same x position, they accumulate to reflect density. Dot color indicates the feature value, with blue representing low values and red representing high values. (b) and (d), SHAP dependence plot showing the relationship between VPD and its SHAP values contributing to GPP_{DT} (b) and GPP_{NT} (d), stratified by the gradient of incoming shortwave radiation (SW). The XGBoost models achieved R^2 values of 0.78 for GPP_{DT} and 0.70 for GPP_{NT} on the held-out validation set.

3.2. VPD threshold effect on NEE

To quantify the critical VPD threshold beyond which the influence of VPD on NEE changes abruptly, as indicated by a marked shift in SHAP values, we applied a three-segment threshold analysis to the SHAP response curve across all forest sites (Fig. 5). When pooling all sites, the first threshold τ_1 was identified at 3.90 hPa (95% CI: 3.87–3.93 hPa), followed by τ_2 at 20.84 hPa (95% CI: 20.59–21.29 hPa). Below τ_1, SHAP values decreased slightly with increasing VPD; between τ_1 and τ_2, they increased rapidly with VPD; and above τ_2, SHAP values continued to increase but at a slower rate. This pattern is broadly consistent with the threshold behavior identified for GPP. The first threshold

https://doi.org/10.5194/egusphere-2026-5126
Preprint. Discussion started: 10 September 2026

299 τ_1 was 6.80 hPa for GPP derived from the daytime partitioning method and 3.96 hPa for GPP derived
300 from the nighttime partitioning method, with corresponding τ_2 at 20.38 hPa and 18.76 hPa,
301 respectively (Fig. S4; Table S2). These results indicate that the effect of VPD on vegetation
302 productivity remains relatively weak below the first threshold, but changes substantially once this
303 threshold is exceeded. Here, τ_1 may indicate the onset of enhanced stomatal regulation under rising
304 atmospheric dryness, beyond which canopy carbon exchange becomes more sensitive to further
305 increases in VPD. Comparable τ_1 were also detected when analyses were conducted for individual
306 forest types, including 3.80 hPa for DBF (Fig. S5a) and 4.53 hPa for ENF (Fig. S5b), as well as
307 when the analysis was repeated using daytime-mean NEE, for which τ_1 was 3.66 hPa (Fig. S1c).

308

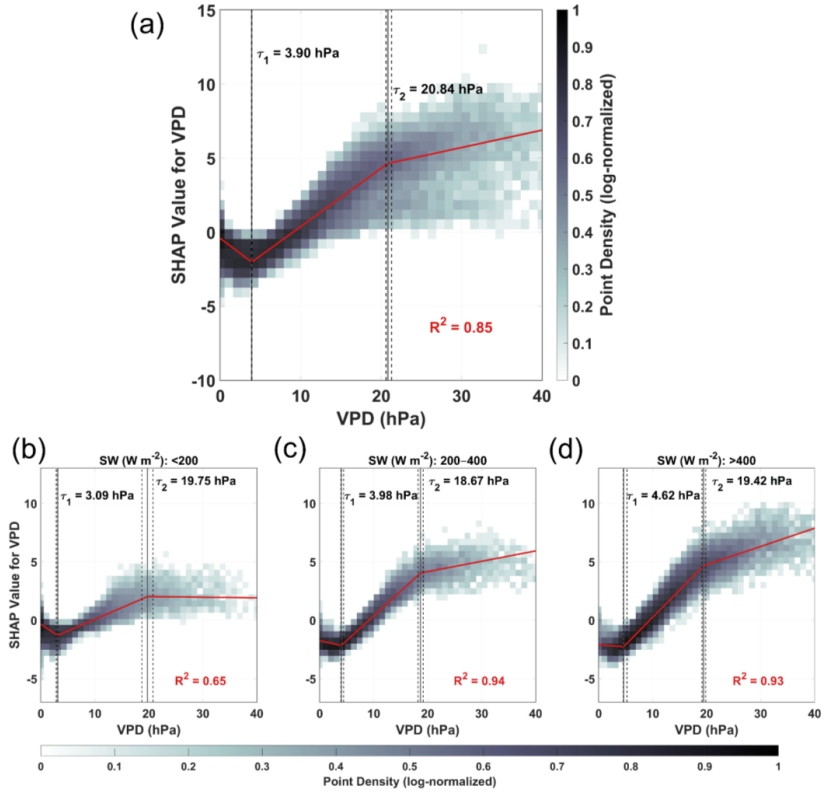

309

https://doi.org/10.5194/egusphere-2026-5126
Preprint. Discussion started: 10 September 2026

Fig. 5. Heatmaps of point density showing the relationship between VPD and the SHAP values of VPD for NEE under different shortwave radiation (SW) conditions: (a) all SW conditions, (b) SW < 200 W m^{-2}, (c) SW between 200 and 400 W m^{-2}, and (d) SW > 400 W m^{-2}. In each panel, color indicates the log-normalized point density within each bin, with darker colors representing higher data concentration. The red curve shows a three-segment continuous piecewise linear fit to the binned median SHAP response. Two thresholds, τ_1 and τ_2, are identified from the fitted response and separate the three response regimes. Solid vertical black lines indicate the estimated thresholds, and dashed vertical black lines indicate their 95% bootstrap confidence intervals. Threshold values are labeled in black. The coefficient of determination (R^2), shown in red, quantifies the fit between the modeled response and the original SHAP values.

Considering the regulatory role of SW in mediating the VPD–NEE relationship, we conducted threshold analyses across all forest sites under different SW conditions (Fig. 5b–c). The threshold τ_1 varied only modestly among SW categories, ranging from 3.09 hPa under low SW conditions (< 200 W m^{-2}) to 4.62 hPa under high SW conditions (> 400 W m^{-2}), with an intermediate value of 3.98 hPa for moderate SW conditions (200–400 W m^{-2}). Across all SW categories, SHAP values for VPD were near zero or slightly negative below τ_1, indicating that VPD exerted only a weak influence on NEE when atmospheric dryness was low. Once VPD exceeded τ_1, SHAP values increased rapidly with increasing VPD, indicating a strengthened positive VPD effect on NEE. The second threshold, τ_2, ranged from 18.67 to 19.75 hPa across SW categories. Notably, the slope of the intermediate segment between τ_1 and τ_2 became steeper under moderate and high SW conditions than under low SW conditions, indicating that stronger radiation amplified the sensitivity of NEE to VPD once τ_1 was exceeded. In addition, SHAP values remained positive at high VPD under strong SW, suggesting that the enhancing effect of VPD on NEE persisted under high-radiation conditions. Together, these results indicate that although the first VPD threshold remained relatively stable across SW conditions, higher SW substantially strengthened the VPD sensitivity of NEE above this threshold.

3.3 Multiple pathways through which environmental variables affect NEE

To further explore the key role of SW in mediating the VPD–NEE relationship, we employed a CB-SEM (Fig. 2) to examine the interrelationships among environmental variables (VPD, SW, TA, and SWC) and NEE under different SW conditions (Fig. 6). Based on the previously identified thresholds, the analysis was restricted to VPD > 5 hPa to exclude conditions with weak atmospheric

https://doi.org/10.5194/egusphere-2026-5126
Preprint. Discussion started: 10 September 2026

dryness stress and to minimize strongly nonlinear responses. Overall, the effects of SW on NEE were relatively limited, because within each SW bin (i.e., each SW interval), SW varied only slightly and was partly constrained by the predefined bin range. However, the effects of TA and VPD on NEE were modulated by SW: as SW increased, the effect of TA on NEE shifted from positive (0.18 for 50–100 W m^{-2}) to negative (−0.44 for 450–500 W m^{-2}), whereas the effect of VPD on NEE strengthened progressively, from −0.01 (for 50–100 W m^{-2}) to 0.64 (for 450–500 W m^{-2}). This pattern is consistent with a stronger regulatory role of SW in shaping the VPD–NEE relationship under high-radiation conditions, although part of the apparent strengthening of the VPD effect may also reflect the intrinsic nonlinear coupling between TA and VPD. Nevertheless, the increase in the VPD effect appears to level off at higher SW levels, suggesting a potential saturation of the SW-mediated modulation of the VPD–NEE relationship.

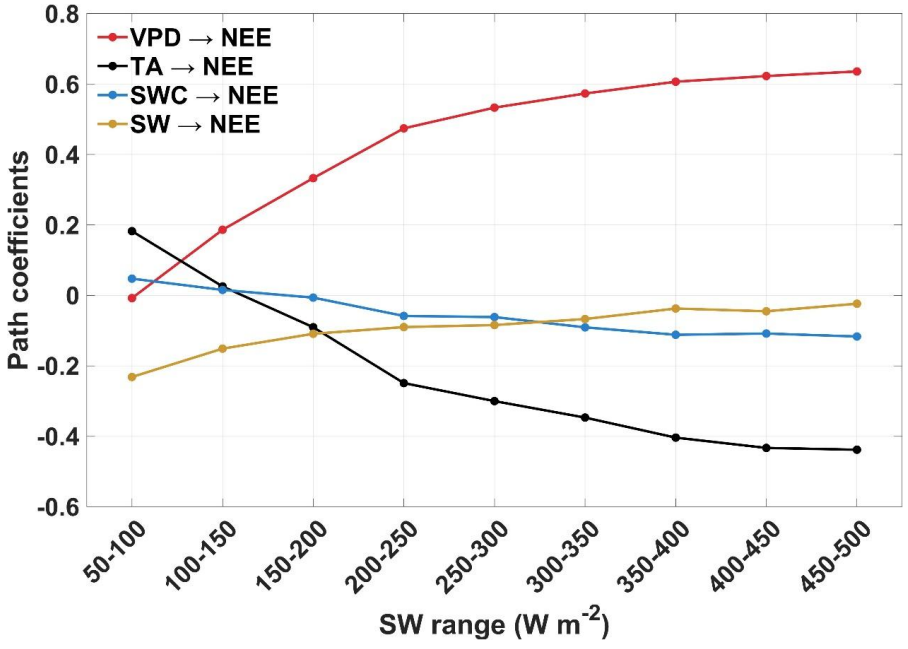

Fig. 6. Path coefficients of environmental variables affecting NEE under different shortwave radiation (SW) conditions derived from the covariance-based structural equation model (CB-SEM) shown in Fig. 2. Positive coefficients indicate positive effects on NEE, whereas negative coefficients indicate negative effects. Each point represents the estimated path coefficient within a given SW bin. All CB-SEM models show strong fits (CFI > 0.99, AGFI > 0.99, RMSEA < 0.01).

https://doi.org/10.5194/egusphere-2026-5126
Preprint. Discussion started: 10 September 2026

3.4 Regulatory role of SW in mediating the VPD–G_s relationship

We therefore analyzed the VPD–G_s relationship under different SW conditions using the nonlinear regression model in Equation (5). The fitted curves represent the expected decline of G_s with increasing VPD, whereas ΔG_s denotes the deviation of the fitted G_s from the mean G_s within each SW bin, highlighting how stomatal regulation responds to atmospheric dryness under different radiation environments. This analysis was restricted to VPD > 5 hPa to minimize potential interference from conditions without atmospheric dryness stress. Our results show that under higher SW conditions, G_s decreases more sharply with increasing VPD (Fig. 7, Fig. S6), indicating stronger stomatal sensitivity to atmospheric dryness. This pattern is also consistent with theoretical expectations derived from the Penman–Monteith framework (Equation 2), which predicts stronger stomatal regulation when evaporative demand is high. Collectively, these findings are consistent with a stomatal mechanism underlying the modulation of the VPD–NEE relationship by SW: high SW amplifies the negative effects of VPD on stomatal conductance, thereby reducing photosynthesis and altering ecosystem carbon exchange.

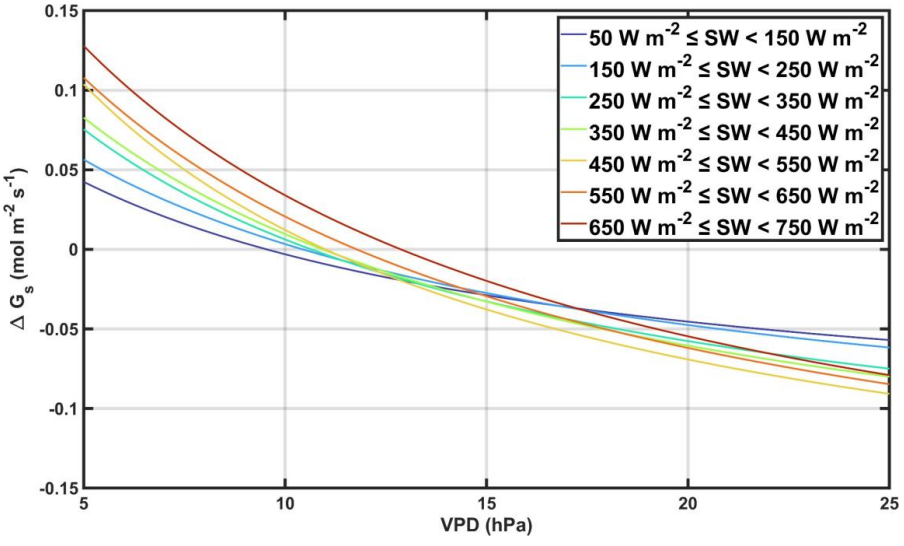

Fig. 7. Relationship between VPD and ΔGs across different shortwave radiation (SW) bins. ΔGs represents the deviation of fitted ecosystem conductance (G_s) from the mean G_s within each SW bin.

https://doi.org/10.5194/egusphere-2026-5126
Preprint. Discussion started: 10 September 2026

The fitted G_s values were obtained using nonlinear least-squares regression of G_s against VPD ($G_s = a/(1 + b \times VPD)$) applied to observations within each SW bin.

4. Discussion

4.1. Dominant role of SW in controlling carbon uptake in forests

Our results highlight the dominant role of SW in regulating forest NEE across Europe, mainly in the following aspects. First, SW emerged as the primary driver of forest carbon uptake explaining nearly 50% of the variability in NEE, GPP_{DT}, and GPP_{NT}. Second, SW mediated the VPD–NEE relationship. Under high SW conditions, VPD imposed stronger constraints on carbon uptake. Higher SW increases net radiation and thus the energy available to supply the latent heat required for evapotranspiration, thereby supporting higher transpiration rates. Under these conditions, elevated environmental VPD is more likely to induce stomatal closure to prevent excessive water loss, which consequently reduces photosynthesis and carbon uptake. In contrast, under low SW, the lower energy available for evapotranspiration reduces transpirational demand and the associated risk of water loss. Consequently, the stomatal limitation induced by elevated VPD may be weaker, resulting in a smaller constraint on photosynthesis and carbon uptake. This ecosystem-scale pattern is also consistent with leaf-level photosynthesis-based stomatal formulations, such as the Ball–Berry (Ball et al., 1987) or Medlyn (Medlyn et al., 2011) models, which imply that the ecosystem impacts of VPD emerge through strong interactions between atmospheric dryness and radiation-driven photosynthetic demand. Such VPD-induced stomatal regulation may be particularly common in forest ecosystems, which generally adopt more conservative water-use strategies than savannas and grasslands. Specifically, trees tend to regulate stomatal opening and reduce transpiration under stress, whereas grasslands often maintain relatively high transpiration rates even during drought conditions (Morgan et al., 2025).

In addition, our path analysis revealed that the effect of TA on NEE was also mediated by SW. After accounting for the relationship between SW and TA, TA exerted a positive effect on NEE when SW was below 200 W m^{-2}, whereas under higher SW conditions (>200 W m^{-2}) the effect became

https://doi.org/10.5194/egusphere-2026-5126
Preprint. Discussion started: 10 September 2026

negative. This shift suggests that under high SW, enhanced photosynthetic activity increases the sensitivity of vegetation carbon uptake to temperature, such that the resulting increase in carbon uptake exceeds the concurrent increase in ecosystem respiration. Notably, the magnitude of the indirect effect of TA on NEE via VPD—calculated as the product of the path coefficient of TA on VPD and that of VPD on NEE—was greater than the direct path coefficient magnitude of TA on NEE under most SW conditions. Since more positive NEE corresponds to weaker net carbon uptake, this indicates that warming-induced increases in VPD, together with direct warming effects, tend to make NEE less negative and thus reduce the carbon sink strength of European forests.

4.2. The effects of VPD change on carbon uptake in forest ecosystems

Based on flux tower observations, we found a generally positive relationship between VPD and NEE, reflecting the well-established negative relationship between VPD and vegetation productivity. At lower VPD levels, however, the NEE response was neutral or even negative, consistent with recent evidence showing that the suppressive effect of VPD on vegetation growth diminishes in humid environments (Chen et al., 2023a; Zhong et al., 2023b; Woodruff et al., 2010). We identified an initial threshold in the VPD effect on NEE at 3.90 hPa, beyond which SHAP values increased rapidly with rising VPD. A second threshold was found at 20.84 hPa, after which SHAP values continued to increase but at a slower rate. The first threshold is consistent with previously reported thresholds (3.5–4.0 hPa) in the VPD-vegetation productivity relationship derived from satellite-based productivity proxies or flux tower-based GPP estimates in high-latitude Eurasia, above which vegetation productivity showed a marked negative response to increasing VPD (Zhong et al., 2023b). This threshold is also below the 5–10 hPa range commonly reported as the minimum VPD at which moisture stress begins to constrain vegetation productivity (Fu et al., 2022; Wang et al., 2022). The second threshold identified at around 20 hPa indicates that although the effect of VPD on NEE continued to strengthen at very high atmospheric dryness, the rate of increase became smaller beyond this point. This pattern is broadly consistent with previous findings that the limiting effects of VPD on light-use efficiency and photosynthesis tend to level off once high VPD conditions are reached (Gao et al., 2022; Grossiord et al., 2020).

https://doi.org/10.5194/egusphere-2026-5126
Preprint. Discussion started: 10 September 2026

It should be noted that the influence of TA was stronger on GPP than on NEE. TA explained 17.1% and 18.5% of the variability in GPP_{DT} and GPP_{NT}, respectively, compared with 7.5% for NEE (Fig. 3). While rising temperature generally stimulates GPP, it also enhances autotrophic and heterotrophic respiration (Chen et al., 2023b), offsetting the photosynthetic gains. Moreover, because GPP is derived from flux tower-observed NEE, both daytime and nighttime partitioning approaches rely heavily on temperature as a key parameter (Reichstein et al., 2005; Lasslop et al., 2010). Such a priori parameterization may overestimate the effects of temperature on GPP and bias threshold detection. For example, in the daytime partitioning approach, the VPD limitation of GPP is set at 10 hPa (Lasslop et al., 2010), below which VPD is assumed to have no effect. As a result, thresholds derived from GPP_{DT} (6.8 hPa) were higher than the 3.90 hPa threshold from the VPD–NEE relationship (Table S2), suggesting a potential underestimation of VPD effects on vegetation productivity and carbon exchange. Therefore, for assessing contributions and detecting thresholds, it is more appropriate to analyze the relationships between measured NEE and climatic drivers (e.g., TA and VPD), rather than relying solely on GPP estimated from empirical models and parameterized relationships.

4.3. Limitations and implications

We acknowledge several uncertainties in this study. First, vegetation responses to climate change are temporally scale-dependent (Novick et al., 2016). Our analysis focused on the sub-daily and daily scale, whereas the dominant drivers and their relative importance may differ at longer temporal scales (e.g., monthly or annual time scale). Such discrepancies could partly arise from time-lag effects between vegetation activities and climatic factors (Lian et al., 2021; Lian et al., 2024), which may vary across biomes and climates (Xu et al., 2022). Moreover, our study considered only climatic drivers, while anthropogenic factors such as management practices and soil nutrient availability (e.g., nitrogen and phosphorus) were not incorporated (Terrer et al., 2019; Wang et al., 2025). Finally, the SEM analyses assumed linear relationships. Compared to non-parametric alternatives such as tree-based machine learning models, linear models are generally more interpretable and better suited for mechanistic understanding, but they may sacrifice predictive accuracy (Li et al., 2025).

https://doi.org/10.5194/egusphere-2026-5126
Preprint. Discussion started: 10 September 2026

More frequent and intense heat periods represent one of the most severe consequences of anthropogenic climate change in Europe (Breil et al., 2023). Global climate models (GCMs) project that rising temperatures and heat extremes will continue over the coming decades (Becker et al., 2022; Li et al., 2021), accompanied by further increases in VPD, with substantial implications for forest functioning. In addition, Europe has also experienced an increase in surface solar radiation—commonly referred to as "brightening" (Wild et al., 2005; Wild, 2009)—since the 1980s, primarily driven by changes in cloud cover and aerosol loading (Wild et al., 2021; Schilliger et al., 2024). GCMs project that this trend will persist through the mid-21st century, particularly in Central and Eastern Europe (Gutiérrez et al., 2020; Hou et al., 2021). Enhanced solar radiation can promote photosynthesis, thereby increasing tree growth and carbon uptake. However, continued "brightening" may also intensify atmospheric water demand: higher solar radiation elevates air temperature, which raises saturated vapor pressure and VPD. In addition, "brightening" contributes to sub-diurnal asymmetric warming, characterized by faster increases in daily maximum than minimum temperature (Zhong et al., 2023a; Huang et al., 2023), further amplifying atmospheric dryness (Zhong et al., 2025b). The concurrent rise in VPD and SW, combined with our finding that VPD exerts stronger constraints on carbon uptake under high SW conditions, suggests a potential risk of reduced carbon sequestration in European forests due to intensifying atmospheric dryness. These findings underscore the urgent need to account for the combined impacts of "brightening" and rising VPD in future projections of forest carbon uptake.

5. Conclusion

Surface SW and VPD in Europe have both increased over recent decades and are projected to continue rising, potentially triggering cascading responses within plants and ecosystems. Using flux tower observations combined with an XGBoost-SHAP framework, supported by threshold and path analyses, our results reveal the following:

(1) SW and VPD are the dominant energy- and water-related drivers that control forest NEE at the half-hourly and daily scale in Europe.

https://doi.org/10.5194/egusphere-2026-5126
Preprint. Discussion started: 10 September 2026

(2) The effect of VPD on NEE exhibits an initial threshold at approximately 3.90 hPa, below which the influence of VPD is neutral or weakly negative, and above which it strengthens rapidly and shifts from negative to positive. A second threshold is detected at approximately 20.84 hPa, beyond which the effect of VPD continues to increase but at a slower rate.

(3) The VPD–NEE relationship is strongly modulated by SW. Under low SW conditions, the effect of VPD increases only weakly after the first threshold is exceeded, whereas under moderate and high SW conditions it strengthens more rapidly. This pattern is consistent with stomatal regulation, as ecosystem conductance declines more sharply with increasing VPD under stronger radiation.

Collectively, these findings suggest that the concurrent rise in SW and VPD may substantially constrain forest productivity and carbon uptake. If ecosystem and Earth system models fail to represent the amplifying effect of shortwave radiation on atmospheric dryness, they may underestimate the synergistic impacts of these climate drivers on forest ecosystems, potentially resulting in overly optimistic projections of forest carbon sequestration. This bias may also influence estimates of mitigation strategies such as bioenergy with carbon capture and storage (BECCS), which rely on sustained biomass production. Future ecosystem modelling and forest management should therefore explicitly consider the interactive effects of SW and VPD, particularly in regions where both drivers are projected to intensify under climate change.

Data availability

All data needed to evaluate the conclusions in the paper are present in the paper and/or the Supplementary Materials. These data are freely accessible from the following sources: The ICOS ecosystem flux and meteorological data were obtained from the ICOS Carbon Portal: Ecosystem final quality (L2) product in ETC-Archive format, release 2025-1 (Icos Ri et al., 2025), DOI: https://doi.org/10.18160/S6HM-CP8Q. The MODIS LAI dataset is from https://doi.org/10.5067/MODIS/MCD15A3H.061.

https://doi.org/10.5194/egusphere-2026-5126
Preprint. Discussion started: 10 September 2026

Author contribution

Z.Z. conceived the study, processed the data, performed the analyses, and wrote the original draft. H.W.C., F.J., and L.L. reviewed and edited the manuscript. H.W.C. coordinated and supervised the project.

Competing interests

The authors declare that they have no conflict of interest.

Acknowledgements

We gratefully acknowledge ICOS RI, the ICOS Ecosystem Thematic Centre, the ICOS Carbon Portal, and all principal investigators and station teams contributing to the ICOS Ecosystem final quality (L2) product in ETC-Archive format, release 2025-1, for providing the ecosystem flux and meteorological data used in this study (DOI: https://doi.org/10.18160/S6HM-CP8Q).

Financial support

The study was supported by internal funding from Chalmers University of Technology. Z.Z was supported by the VAPOR project (grant number 101154385), funded by the Horizon Europe, MSCA Postdoctoral Fellowships 2023.

References

Ball, J. T., Woodrow, I. E., and Berry, J. A.: A Model Predicting Stomatal Conductance and its Contribution to the Control of Photosynthesis under Different Environmental Conditions, in: Progress in Photosynthesis Research: Volume 4 Proceedings of the VIIth International Congress on Photosynthesis Providence, Rhode Island, USA, August 10–15, 1986, edited by: Biggins, J., Springer Netherlands, Dordrecht, 221-224, 10.1007/978-94-017-0519-6_48, 1987.

Becker, F. N., Fink, A. H., Bissolli, P., and Pinto, J. G.: Towards a more comprehensive assessment of

https://doi.org/10.5194/egusphere-2026-5126
Preprint. Discussion started: 10 September 2026

the intensity of historical European heat waves (1979–2019), Atmospheric Science Letters, 23, e1120, https://doi.org/10.1002/asl.1120, 2022.

Beloiu, M., Stahlmann, R., and Beierkuhnlein, C.: Drought impacts in forest canopy and deciduous tree saplings in Central European forests, Forest Ecology and Management, 509, 120075, https://doi.org/10.1016/j.foreco.2022.120075, 2022.

Bois, B., Pieri, P., Van Leeuwen, C., Wald, L., Huard, F., Gaudillere, J. P., and Saur, E.: Using remotely sensed solar radiation data for reference evapotranspiration estimation at a daily time step, Agricultural and Forest Meteorology, 148, 619-630, https://doi.org/10.1016/j.agrformet.2007.11.005, 2008.

Breil, M., Weber, A., and Pinto, J. G.: The potential of an increased deciduous forest fraction to mitigate the effects of heat extremes in Europe, Biogeosciences, 20, 2237-2250, 10.5194/bg-20-2237-2023, 2023.

Buck, A. L.: New Equations for Computing Vapor Pressure and Enhancement Factor, Journal of Applied Meteorology and Climatology, 20, 1527-1532, https://doi.org/10.1175/1520-0450(1981)020<1527:NEFCVP>2.0.CO;2, 1981.

Carnicer, J., Coll, M., Ninyerola, M., Pons, X., Sánchez, G., and Peñuelas, J.: Widespread crown condition decline, food web disruption, and amplified tree mortality with increased climate change-type drought, Proc. Natl. Acad. Sci., 108, 1474-1478, doi:10.1073/pnas.1010070108, 2011.

Chen, N., Zhang, Y., Yuan, F., Song, C., Xu, M., Wang, Q., Hao, G., Bao, T., Zuo, Y., Liu, J., Zhang, T., Song, Y., Sun, L., Guo, Y., Zhang, H., Ma, G., Du, Y., Xu, X., and Wang, X.: Warming-induced vapor pressure deficit suppression of vegetation growth diminished in northern peatlands, Nat. Commun., 14, 7885, 10.1038/s41467-023-42932-w, 2023a.

Chen, T. and Guestrin, C.: XGBoost: A Scalable Tree Boosting System, Proceedings of the 22nd ACM SIGKDD International Conference on Knowledge Discovery and Data Mining, San Francisco, California, USA, 10.1145/2939672.2939785, 2016.

Chen, W., Wang, S., Wang, J., Xia, J., Luo, Y., Yu, G., and Niu, S.: Evidence for widespread thermal optimality of ecosystem respiration, Nat. Ecol. Evol., 7, 1379-1387, 10.1038/s41559-023-02121-w, 2023b.

Ciais, P., Reichstein, M., Viovy, N., Granier, A., Ogée, J., Allard, V., Aubinet, M., Buchmann, N., Bernhofer, C., Carrara, A., Chevallier, F., De Noblet, N., Friend, A. D., Friedlingstein, P., Grünwald, T., Heinesch, B., Keronen, P., Knohl, A., Krinner, G., Loustau, D., Manca, G., Matteucci, G., Miglietta, F., Ourcival, J. M., Papale, D., Pilegaard, K., Rambal, S., Seufert, G., Soussana, J. F., Sanz, M. J., Schulze, E. D., Vesala, T., and Valentini, R.: Europe-wide reduction in primary productivity caused by the heat and drought in 2003, Nature, 437, 529-533, 10.1038/nature03972, 2005.

Dai, A., Trenberth, K. E., and Karl, T. R.: Effects of Clouds, Soil Moisture, Precipitation, and Water Vapor on Diurnal Temperature Range, J. Clim., 12, 2451-2473, https://doi.org/10.1175/1520-0442(1999)012<2451:EOCSMP>2.0.CO;2, 1999.

Donohue, R. J., McVicar, T. R., and Roderick, M. L.: Assessing the ability of potential evaporation formulations to capture the dynamics in evaporative demand within a changing climate, J. Hydrol., 386, 186-197, https://doi.org/10.1016/j.jhydrol.2010.03.020, 2010.

Ek, M. B. and Holtslag, A. A. M.: Influence of Soil Moisture on Boundary Layer Cloud Development, J. Hydrometeorol., 5, 86-99, https://doi.org/10.1175/1525-7541(2004)005<0086:IOSMOB>2.0.CO;2, 2004.

Fang, Z., Zhang, W., Brandt, M., Abdi, A. M., and Fensholt, R.: Globally Increasing Atmospheric

https://doi.org/10.5194/egusphere-2026-5126
Preprint. Discussion started: 10 September 2026

Aridity Over the 21st Century, Earth's Future, 10, e2022EF003019, https://doi.org/10.1029/2022EF003019, 2022.

Fu, Z., Ciais, P., Prentice, I. C., Gentine, P., Makowski, D., Bastos, A., Luo, X., Green, J. K., Stoy, P. C., Yang, H., and Hajima, T.: Atmospheric dryness reduces photosynthesis along a large range of soil water deficits, Nat. Commun., 13, 989, 10.1038/s41467-022-28652-7, 2022.

Fu, Z., Ciais, P., Bastos, A., Stoy, P. C., Yang, H., Green, J. K., Wang, B., Yu, K., Huang, Y., Knohl, A., Šigut, L., Gharun, M., Cuntz, M., Arriga, N., Roland, M., Peichl, M., Migliavacca, M., Cremonese, E., Varlagin, A., Brümmer, C., Gourlez de la Motte, L., Fares, S., Buchmann, N., El-Madany, T. S., Pitacco, A., Vendrame, N., Li, Z., Vincke, C., Magliulo, E., and Koebsch, F.: Sensitivity of gross primary productivity to climatic drivers during the summer drought of 2018 in Europe, Philosophical Transactions of the Royal Society B: Biological Sciences, 375, 20190747, doi:10.1098/rstb.2019.0747, 2020.

Gao, D., Wang, S., Li, Z., Wei, F., Chen, P., Song, S., Wang, Y., Wang, L., and Fu, B.: Threshold of vapour–pressure deficit constraint on light use efficiency varied with soil water content, Ecohydrology, 15, e2305, https://doi.org/10.1002/eco.2305, 2022.

Gebrechorkos, S. H., Sheffield, J., Vicente-Serrano, S. M., Funk, C., Miralles, D. G., Peng, J., Dyer, E., Talib, J., Beck, H. E., Singer, M. B., and Dadson, S. J.: Warming accelerates global drought severity, Nature, 642, 628-635, 10.1038/s41586-025-09047-2, 2025.

Grossiord, C., Buckley, T. N., Cernusak, L. A., Novick, K. A., Poulter, B., Siegwolf, R. T. W., Sperry, J. S., and McDowell, N. G.: Plant responses to rising vapor pressure deficit, New Phytol., 226, 1550-1566, https://doi.org/10.1111/nph.16485, 2020.

Gutiérrez, C., Somot, S., Nabat, P., Mallet, M., Corre, L., Meijgaard, E. v., Perpiñán, O., and Gaertner, M. Á.: Future evolution of surface solar radiation and photovoltaic potential in Europe: investigating the role of aerosols, Environmental Research Letters, 15, 034035, 10.1088/1748-9326/ab6666, 2020.

Hartmann, H. and Trumbore, S.: Understanding the roles of nonstructural carbohydrates in forest trees – from what we can measure to what we want to know, New Phytol., 211, 386-403, https://doi.org/10.1111/nph.13955, 2016.

He, B., Chen, C., Lin, S., Yuan, W., Chen, H. W., Chen, D., Zhang, Y., Guo, L., Zhao, X., Liu, X., Piao, S., Zhong, Z., Wang, R., and Tang, R.: Worldwide impacts of atmospheric vapor pressure deficit on the interannual variability of terrestrial carbon sinks, Natl. Sci. Rev., 9, 10.1093/nsr/nwab150, 2021.

Hou, X., Wild, M., Folini, D., Kazadzis, S., and Wohland, J.: Climate change impacts on solar power generation and its spatial variability in Europe based on CMIP6, Earth Syst. Dynam., 12, 1099-1113, 10.5194/esd-12-1099-2021, 2021.

Huang, M., Piao, S., Ciais, P., Peñuelas, J., Wang, X., Keenan, T. F., Peng, S., Berry, J. A., Wang, K., Mao, J., Alkama, R., Cescatti, A., Cuntz, M., De Deurwaerder, H., Gao, M., He, Y., Liu, Y., Luo, Y., Myneni, R. B., Niu, S., Shi, X., Yuan, W., Verbeeck, H., Wang, T., Wu, J., and Janssens, I. A.: Air temperature optima of vegetation productivity across global biomes, Nat. Ecol. Evol., 3, 772-779, 10.1038/s41559-019-0838-x, 2019.

Huang, X., Dunn, R. J. H., Li, L. Z. X., McVicar, T. R., Azorin-Molina, C., and Zeng, Z.: Increasing Global Terrestrial Diurnal Temperature Range for 1980–2021, Geophys. Res. Lett., 50, e2023GL103503, https://doi.org/10.1029/2023GL103503, 2023.

ICOS RI, Aalto, J., Aalto, P., Aaltonen, H., ..., and Šlížek, J.: Ecosystem final quality (L2) product in ETC-Archive format - release 2025-1, ICOS ERIC -- Carbon Portal, 10.18160/S6HM-CP8Q, 2025.

https://doi.org/10.5194/egusphere-2026-5126
Preprint. Discussion started: 10 September 2026

Jeong, J.-H., Kug, J.-S., Kim, B.-M., Min, S.-K., Linderholm, H. W., Ho, C.-H., Rayner, D., Chen, D., and Jun, S.-Y.: Greening in the circumpolar high-latitude may amplify warming in the growing season, Climate Dynamics, 38, 1421-1431, 10.1007/s00382-011-1142-x, 2012.

Kašpar, J., Krůček, M., and Král, K.: The effects of solar radiation on daily and seasonal stem increment of canopy trees in European temperate old-growth forests, New Phytol., 243, 662-673, https://doi.org/10.1111/nph.19852, 2024.

Körner, C.: Carbon limitation in trees, J. Ecol., 91, 4-17, https://doi.org/10.1046/j.1365-2745.2003.00742.x, 2003.

Lasslop, G., Reichstein, M., Papale, D., Richardson, A. D., Arneth, A., Barr, A., Stoy, P., and Wohlfahrt, G.: Separation of net ecosystem exchange into assimilation and respiration using a light response curve approach: critical issues and global evaluation, Global Change Biol., 16, 187-208, https://doi.org/10.1111/j.1365-2486.2009.02041.x, 2010.

Lendzion, J. and Leuschner, C.: Growth of European beech (Fagus sylvatica L.) saplings is limited by elevated atmospheric vapour pressure deficits, Forest Ecology and Management, 256, 648-655, https://doi.org/10.1016/j.foreco.2008.05.008, 2008.

Li, C., Zwiers, F., Zhang, X., Li, G., Sun, Y., and Wehner, M.: Changes in Annual Extremes of Daily Temperature and Precipitation in CMIP6 Models, J. Clim., 34, 3441-3460, https://doi.org/10.1175/JCLI-D-19-1013.1, 2021.

Li, Y., Schuldt, A., Bauhus, J., Belluau, M., Berthelot, S., Burghardt, K. T., Bruelheide, H., Castagneyrol, B., Chu, C., Eisenhauer, N., Ferlian, O., Fründ, J., Gebauer, T., Gravel, D., Jactel, H., Li, S., Liang, Y., Parker, J. D., Parker, W. C., Scherer-Lorenzen, M., Staab, M., Verheyen, K., Schmid, B., Ma, K., and Liu, X.: The tree growth–herbivory relationship depends on functional traits across forest biodiversity experiments, Nat. Ecol. Evol., 10.1038/s41559-025-02835-z, 2025.

Lian, X., Peñuelas, J., Ryu, Y., Piao, S., Keenan, T. F., Fang, J., Yu, K., Chen, A., Zhang, Y., and Gentine, P.: Diminishing carryover benefits of earlier spring vegetation growth, Nat. Ecol. Evol., 8, 218-228, 10.1038/s41559-023-02272-w, 2024.

Lian, X., Piao, S., Chen, A., Wang, K., Li, X., Buermann, W., Huntingford, C., Peñuelas, J., Xu, H., and Myneni, R. B.: Seasonal biological carryover dominates northern vegetation growth, Nat. Commun., 12, 983, 10.1038/s41467-021-21223-2, 2021.

Lin, C., Gentine, P., Huang, Y., Guan, K., Kimm, H., and Zhou, S.: Diel ecosystem conductance response to vapor pressure deficit is suboptimal and independent of soil moisture, Agricultural and Forest Meteorology, 250-251, 24-34, https://doi.org/10.1016/j.agrformet.2017.12.078, 2018.

Lin, S., Chen, X., Xia, J., Xin, Q., Fu, Z., He, B., Liu, Q., Piao, S., and Yuan, W.: Global vegetation production may decrease in this century due to rising atmospheric dryness, Nat. Ecol. Evol., 9, 2279-2289, 10.1038/s41559-025-02885-3, 2025.

Lindner, M., Maroschek, M., Netherer, S., Kremer, A., Barbati, A., Garcia-Gonzalo, J., Seidl, R., Delzon, S., Corona, P., Kolström, M., Lexer, M. J., and Marchetti, M.: Climate change impacts, adaptive capacity, and vulnerability of European forest ecosystems, Forest Ecology and Management, 259, 698-709, https://doi.org/10.1016/j.foreco.2009.09.023, 2010.

Liu, L., Gudmundsson, L., Hauser, M., Qin, D., Li, S., and Seneviratne, S. I.: Soil moisture dominates dryness stress on ecosystem production globally, Nat. Commun., 11, 4892, 10.1038/s41467-020-18631-1, 2020.

Lundberg, S. M., Erion, G., Chen, H., DeGrave, A., Prutkin, J. M., Nair, B., Katz, R., Himmelfarb, J., Bansal, N., and Lee, S.-I.: From local explanations to global understanding with explainable AI for

https://doi.org/10.5194/egusphere-2026-5126
Preprint. Discussion started: 10 September 2026

trees, Nature Machine Intelligence, 2, 56-67, 10.1038/s42256-019-0138-9, 2020.
Marquardt, D. W.: An algorithm for least-squares estimation of nonlinear parameters, Journal of the society for Industrial and Applied Mathematics, 11, 431-441, 1963.
McDowell, N., Allen, C. D., Anderson-Teixeira, K., Brando, P., Brienen, R., Chambers, J., Christoffersen, B., Davies, S., Doughty, C., Duque, A., Espirito-Santo, F., Fisher, R., Fontes, C. G., Galbraith, D., Goodsman, D., Grossiord, C., Hartmann, H., Holm, J., Johnson, D. J., Kassim, A. R., Keller, M., Koven, C., Kueppers, L., Kumagai, T. o., Malhi, Y., McMahon, S. M., Mencuccini, M., Meir, P., Moorcroft, P., Muller-Landau, H. C., Phillips, O. L., Powell, T., Sierra, C. A., Sperry, J., Warren, J., Xu, C., and Xu, X.: Drivers and mechanisms of tree mortality in moist tropical forests, New Phytol., 219, 851-869, https://doi.org/10.1111/nph.15027, 2018.
Medlyn, B. E., Duursma, R. A., Eamus, D., Ellsworth, D. S., Prentice, I. C., Barton, C. V. M., Crous, K. Y., De Angelis, P., Freeman, M., and Wingate, L.: Reconciling the optimal and empirical approaches to modelling stomatal conductance, Global Change Biol., 17, 2134-2144, https://doi.org/10.1111/j.1365-2486.2010.02375.x, 2011.
Mokhtari, A., Noory, H., and Vazifedoust, M.: Performance of Different Surface Incoming Solar Radiation Models and Their Impacts on Reference Evapotranspiration, Water Resources Management, 32, 3053-3070, 10.1007/s11269-018-1974-9, 2018.
Morgan, B. E., Araki, R., Trugman, A. T., and Caylor, K. K.: Ecological and hydroclimatic determinants of vegetation water-use strategies, Nat. Ecol. Evol., 10.1038/s41559-025-02810-8, 2025.
Murray, F. W.: On the Computation of Saturation Vapor Pressure, Journal of Applied Meteorology and Climatology, 6, 203-204, https://doi.org/10.1175/1520-0450(1967)006<0203:OTCOSV>2.0.CO;2, 1967.
Myneni, R., Knyazikhin, Y., and Park, T.: MOD15A2H MODIS/Terra leaf area Index/FPAR 8-Day L4 global 500m SIN grid V006, NASA EOSDIS Land Processes Distributed Active Archive Center (DAAC) data set, MOD15A12H. 006, 2015.
Novick, K. A., Ficklin, D. L., Stoy, P. C., Williams, C. A., Bohrer, G., Oishi, A. C., Papuga, S. A., Blanken, P. D., Noormets, A., Sulman, B. N., Scott, R. L., Wang, L., and Phillips, R. P.: The increasing importance of atmospheric demand for ecosystem water and carbon fluxes, Nat. Clim. Change, 6, 1023-1027, 10.1038/nclimate3114, 2016.
Patacca, M., Lindner, M., Lucas-Borja, M. E., Cordonnier, T., Fidej, G., Gardiner, B., Hauf, Y., Jasinevičius, G., Labonne, S., Linkevičius, E., Mahnken, M., Milanovic, S., Nabuurs, G.-J., Nagel, T. A., Nikinmaa, L., Panyatov, M., Bercak, R., Seidl, R., Ostrogović Sever, M. Z., Socha, J., Thom, D., Vuletic, D., Zudin, S., and Schelhaas, M.-J.: Significant increase in natural disturbance impacts on European forests since 1950, Global Change Biol., 29, 1359-1376, https://doi.org/10.1111/gcb.16531, 2023.
Pearcy, R. W., Schulze, E. D., and Zimmermann, R.: Measurement of transpiration and leaf conductance, in: Plant Physiological Ecology: Field methods and instrumentation, edited by: Pearcy, R. W., Ehleringer, J. R., Mooney, H. A., and Rundel, P. W., Springer Netherlands, Dordrecht, 137-160, 10.1007/978-94-009-2221-1_8, 1989.
Penman, H. and Long, I.: Vegetation and Hydrology, Commonwealth Bureau of Soils Tech, 1963.
Penman, H. L.: Natural evaporation from open water, bare soil and grass, Proceedings of the Royal Society of London A: Mathematical, Physical and Engineering Sciences, 120-145,
Pfeifroth, U., Sanchez-Lorenzo, A., Manara, V., Trentmann, J., and Hollmann, R.: Trends and Variability of Surface Solar Radiation in Europe Based On Surface- and Satellite-Based Data Records, J. Geophys. Res.:Atmos., 123, 1735-1754, https://doi.org/10.1002/2017JD027418, 2018.

https://doi.org/10.5194/egusphere-2026-5126
Preprint. Discussion started: 10 September 2026

Piao, S., Ciais, P., Friedlingstein, P., Peylin, P., Reichstein, M., Luyssaert, S., Margolis, H., Fang, J., Barr, A., Chen, A., Grelle, A., Hollinger, D. Y., Laurila, T., Lindroth, A., Richardson, A. D., and Vesala, T.: Net carbon dioxide losses of northern ecosystems in response to autumn warming, Nature, 451, 49-52, 10.1038/nature06444, 2008.

Reichstein, M., Falge, E., Baldocchi, D., Papale, D., Aubinet, M., Berbigier, P., Bernhofer, C., Buchmann, N., Gilmanov, T., Granier, A., Grünwald, T., Havránková, K., Ilvesniemi, H., Janous, D., Knohl, A., Laurila, T., Lohila, A., Loustau, D., Matteucci, G., Meyers, T., Miglietta, F., Ourcival, J.-M., Pumpanen, J., Rambal, S., Rotenberg, E., Sanz, M., Tenhunen, J., Seufert, G., Vaccari, F., Vesala, T., Yakir, D., and Valentini, R.: On the separation of net ecosystem exchange into assimilation and ecosystem respiration: review and improved algorithm, Global Change Biol., 11, 1424-1439, https://doi.org/10.1111/j.1365-2486.2005.001002.x, 2005.

Rossi, S., Anfodillo, T., Čufar, K., Cuny, H. E., Deslauriers, A., Fonti, P., Frank, D., Gričar, J., Gruber, A., Huang, J.-G., Jyske, T., Kašpar, J., King, G., Krause, C., Liang, E., Mäkinen, H., Morin, H., Nöjd, P., Oberhuber, W., Prislan, P., Rathgeber, C. B. K., Saracino, A., Swidrak, I., and Treml, V.: Pattern of xylem phenology in conifers of cold ecosystems at the Northern Hemisphere, Global Change Biol., 22, 3804-3813, https://doi.org/10.1111/gcb.13317, 2016.

Sanchez-Lorenzo, A., Enriquez-Alonso, A., Wild, M., Trentmann, J., Vicente-Serrano, S. M., Sanchez-Romero, A., Posselt, R., and Hakuba, M. Z.: Trends in downward surface solar radiation from satellites and ground observations over Europe during 1983–2010, Remote Sens. Environ., 189, 108-117, https://doi.org/10.1016/j.rse.2016.11.018, 2017.

Sanginés de Cárcer, P., Vitasse, Y., Peñuelas, J., Jassey, V. E. J., Buttler, A., and Signarbieux, C.: Vapor–pressure deficit and extreme climatic variables limit tree growth, Global Change Biol., 24, 1108-1122, https://doi.org/10.1111/gcb.13973, 2018.

Schilliger, L., Tetzlaff, A., Bourgeois, Q., Correa, L. F., and Wild, M.: An Investigation on Causes of the Detected Surface Solar Radiation Brightening in Europe Using Satellite Data, J. Geophys. Res.:Atmos., 129, e2024JD041101, https://doi.org/10.1029/2024JD041101, 2024.

Seidl, R., Schelhaas, M.-J., Rammer, W., and Verkerk, P. J.: Increasing forest disturbances in Europe and their impact on carbon storage, Nat. Clim. Change, 4, 806-810, 10.1038/nclimate2318, 2014.

Seneviratne, S. I., Corti, T., Davin, E. L., Hirschi, M., Jaeger, E. B., Lehner, I., Orlowsky, B., and Teuling, A. J.: Investigating soil moisture–climate interactions in a changing climate: A review, Earth-Science Reviews, 99, 125-161, https://doi.org/10.1016/j.earscirev.2010.02.004, 2010.

Senf, C. and Seidl, R.: Mapping the forest disturbance regimes of Europe, Nature Sustainability, 4, 63-70, 10.1038/s41893-020-00609-y, 2021.

Senf, C., Buras, A., Zang, C. S., Rammig, A., and Seidl, R.: Excess forest mortality is consistently linked to drought across Europe, Nat. Commun., 11, 6200, 10.1038/s41467-020-19924-1, 2020.

Song, Y., Jiao, W., Wang, J., and Wang, L.: Increased Global Vegetation Productivity Despite Rising Atmospheric Dryness Over the Last Two Decades, Earth's Future, 10, e2021EF002634, https://doi.org/10.1029/2021EF002634, 2022.

Stanhill, G. and Cohen, S.: Global dimming: a review of the evidence for a widespread and significant reduction in global radiation with discussion of its probable causes and possible agricultural consequences, Agricultural and Forest Meteorology, 107, 255-278, https://doi.org/10.1016/S0168-1923(00)00241-0, 2001.

Stocker, B. D., Zscheischler, J., Keenan, T. F., Prentice, I. C., Peñuelas, J., and Seneviratne, S. I.: Quantifying soil moisture impacts on light use efficiency across biomes, New Phytol., 218, 1430-

https://doi.org/10.5194/egusphere-2026-5126
Preprint. Discussion started: 10 September 2026

1449, https://doi.org/10.1111/nph.15123, 2018.
Terrer, C., Jackson, R. B., Prentice, I. C., Keenan, T. F., Kaiser, C., Vicca, S., Fisher, J. B., Reich, P. B., Stocker, B. D., Hungate, B. A., Peñuelas, J., McCallum, I., Soudzilovskaia, N. A., Cernusak, L. A., Talhelm, A. F., Van Sundert, K., Piao, S., Newton, P. C. D., Hovenden, M. J., Blumenthal, D. M., Liu, Y. Y., Müller, C., Winter, K., Field, C. B., Viechtbauer, W., Van Lissa, C. J., Hoosbeek, M. R., Watanabe, M., Koike, T., Leshyk, V. O., Polley, H. W., and Franklin, O.: Nitrogen and phosphorus constrain the CO2 fertilization of global plant biomass, Nat. Clim. Change, 9, 684-689, 10.1038/s41558-019-0545-2, 2019.
Trotsiuk, V., Babst, F., Grossiord, C., Gessler, A., Forrester, D. I., Buchmann, N., Schaub, M., and Eugster, W.: Tree growth in Switzerland is increasingly constrained by rising evaporative demand, J. Ecol., 109, 2981-2990, https://doi.org/10.1111/1365-2745.13712, 2021.
van der Woude, A. M., Peters, W., Joetzjer, E., Lafont, S., Koren, G., Ciais, P., Ramonet, M., Xu, Y., Bastos, A., Botía, S., Sitch, S., de Kok, R., Kneuer, T., Kubistin, D., Jacotot, A., Loubet, B., Herig-Coimbra, P.-H., Loustau, D., and Luijkx, I. T.: Temperature extremes of 2022 reduced carbon uptake by forests in Europe, Nat. Commun., 14, 6218, 10.1038/s41467-023-41851-0, 2023.
Wang, H., Yan, S., Ciais, P., Wigneron, J.-P., Liu, L., Li, Y., Fu, Z., Ma, H., Liang, Z., Wei, F., Wang, Y., and Li, S.: Exploring complex water stress–gross primary production relationships: Impact of climatic drivers, main effects, and interactive effects, Global Change Biol., 28, 4110-4123, https://doi.org/10.1111/gcb.16201, 2022.
Wang, L., Tian, F., Han, S., and Wei, Z.: Determinants of the Asymmetric Parameter in the Generalized Complementary Principle of Evaporation, Water Resources Research, 56, e2019WR026570, https://doi.org/10.1029/2019WR026570, 2020.
Wang, S., Ciais, P., Reich, P. B., Cescatti, A., Ellsworth, D. S., Janssens, I. A., Sardans, J., Luo, Y., Smith, N. G., Du, E., Tian, D., Jiang, Y., Ding, Y., and Peñuelas, J.: Phosphorus constrains global photosynthesis more than nitrogen does, Nat. Ecol. Evol., 10.1038/s41559-025-02842-0, 2025.
Way, D. A. and Yamori, W.: Thermal acclimation of photosynthesis: on the importance of adjusting our definitions and accounting for thermal acclimation of respiration, Photosynth Res, 119, 89-100, 10.1007/s11120-013-9873-7, 2014.
Wild, M.: Global dimming and brightening: A review, J. Geophys. Res.:Atmos., 114, 2009.
Wild, M., Wacker, S., Yang, S., and Sanchez-Lorenzo, A.: Evidence for Clear-Sky Dimming and Brightening in Central Europe, Geophys. Res. Lett., 48, e2020GL092216, https://doi.org/10.1029/2020GL092216, 2021.
Wild, M., Gilgen, H., Roesch, A., Ohmura, A., Long, C. N., Dutton, E. G., Forgan, B., Kallis, A., Russak, V., and Tsvetkov, A.: From Dimming to Brightening: Decadal Changes in Solar Radiation at Earth's Surface, Science, 308, 847-850, 10.1126/science.1103215, 2005.
Woodruff, D. R., Meinzer, F. C., and McCulloh, K. A.: Height-related trends in stomatal sensitivity to leaf-to-air vapour pressure deficit in a tall conifer, Journal of Experimental Botany, 61, 203-210, 10.1093/jxb/erp291, 2010.
Wu, T., Tissue, D. T., Jiang, M., Slot, M., Crous, K. Y., Yuan, J., Liu, J., Jin, S., Wu, C., Deng, Y., Huang, C., Shi, F., Fang, X., Li, R., and Mao, R.: Leaf Photosynthetic and Respiratory Thermal Acclimation in Terrestrial Plants in Response to Warming: A Global Synthesis, Global Change Biol., 31, e70026, https://doi.org/10.1111/gcb.70026, 2025.
Xie, J., Yin, G., Xie, Q., Wu, C., Yuan, W., Zeng, Y., Verger, A., Descals, A., Filella, I., and Peñuelas, J.: Shifts in Climatic Limitations on Global Vegetation Productivity Unveiled by Shapley Additive

https://doi.org/10.5194/egusphere-2026-5126
Preprint. Discussion started: 10 September 2026

Explanation: Reduced Temperature but Increased Water Limitations, J. Geophys. Res.:Biogeosci., 129, e2024JG008354, https://doi.org/10.1029/2024JG008354, 2024.

Xu, S., Gentine, P., Li, L., Wang, L., Yu, Z., Dong, N., Ju, Q., and Zhang, Y.: Response of Ecosystem Productivity to High Vapor Pressure Deficit and Low Soil Moisture: Lessons Learned From the Global Eddy-Covariance Observations, Earth's Future, 11, e2022EF003252, https://doi.org/10.1029/2022EF003252, 2023a.

Xu, S., Lettenmaier, D. P., McVicar, T. R., Gentine, P., Beck, H. E., Fisher, J. B., Yu, Z., Dong, N., Koppa, A., and McCabe, M. F.: Increasing atmospheric evaporative demand across the Tibetan plateau and implications for surface water resources, iScience, 28, 10.1016/j.isci.2024.111623, 2025.

Xu, S., McVicar, T. R., Li, L., Yu, Z., Jiang, P., Zhang, Y., Ban, Z., Xing, W., Dong, N., Zhang, H., and Zhang, M.: Globally assessing the hysteresis between sub-diurnal actual evaporation and vapor pressure deficit at the ecosystem scale: Patterns and mechanisms, Agricultural and Forest Meteorology, 323, 109085, https://doi.org/10.1016/j.agrformet.2022.109085, 2022.

Xu, Z., Man, X., Hou, Y., Shang, Y., and Cai, T.: Canopy transpiration and its controlling mechanisms among rainfall patterns in a boreal larch forest in China, J. Hydrol., 625, 130041, https://doi.org/10.1016/j.jhydrol.2023.130041, 2023b.

Yuan, W., Zheng, Y., Piao, S., Ciais, P., and Yang, S.: Increased atmospheric vapor pressure deficit reduces global vegetation growth, Sci. Adv., 5, eaax1396, 10.1126/sciadv.aax1396, 2019.

Zhang, W., Luo, G., Hamdi, R., Ma, X., Termonia, P., and De Maeyer, P.: Drought changes the dominant water stress on the grassland and forest production in the northern hemisphere, Agricultural and Forest Meteorology, 345, 109831, https://doi.org/10.1016/j.agrformet.2023.109831, 2024.

Zhong, Z., Chen, H. W., He, B., and Su, B.: Contrasting vegetation productivity responses in arid and humid zones to recent changes in diurnal temperature range, The Innovation Geoscience, 100163, 10.59717/j.xinn-geo.2025.100163, 2025a.

Zhong, Z., Chen, H. W., Dai, A., Zhou, T., He, B., and Su, B.: Sub-diurnal asymmetric warming has amplified atmospheric dryness since the 1980s, Nat. Commun., 16, 8247, 10.1038/s41467-025-63672-z, 2025b.

Zhong, Z., He, B., Chen, H. W., Chen, D., Zhou, T., Dong, W., Xiao, C., Xie, S.-p., Song, X., Guo, L., Ding, R., Zhang, L., Huang, L., Yuan, W., Hao, X., Ji, D., and Zhao, X.: Reversed asymmetric warming of sub-diurnal temperature over land during recent decades, Nat. Commun., 14, 7189, 10.1038/s41467-023-43007-6, 2023a.

Zhong, Z., He, B., Wang, Y.-P., Chen, H. W., Chen, D., Fu, Y. H., Chen, Y., Guo, L., Deng, Y., Huang, L., Yuan, W., Hao, X., Tang, R., Liu, H., Sun, L., Xie, X., and Zhang, Y.: Disentangling the effects of vapor pressure deficit on northern terrestrial vegetation productivity, Sci. Adv., 9, eadf3166, doi:10.1126/sciadv.adf3166, 2023b.

Zhou, S., Zhang, Y., Park Williams, A., and Gentine, P.: Projected increases in intensity, frequency, and terrestrial carbon costs of compound drought and aridity events, Science Advances, 5, eaau5740, 10.1126/sciadv.aau5740, 2019.